

Graph-Structured Multi-task Regression and an Efficient Optimization Method for General Fused Lasso

Xi Chen¹ Seyoung Kim¹ Qihang Lin²
Jaime G. Carbonell¹ Eric P. Xing¹ *

¹ School of Computer Science

² Tepper School of Business

Carnegie Mellon University

Pittsburgh, PA 15213

Abstract

We consider the problem of learning a structured multi-task regression, where the output consists of multiple responses that are related by a graph and the correlated response variables are dependent on the common inputs in a sparse but synergistic manner. Previous methods such as ℓ_1/ℓ_2 -regularized multi-task regression assume that all of the output variables are equally related to the inputs, although in many real-world problems, outputs are related in a complex manner. In this paper, we propose graph-guided fused lasso (GFlasso) for structured multi-task regression that exploits the graph structure over the output variables. We introduce a novel penalty function based on fusion penalty to encourage highly correlated outputs to share a common set of relevant inputs. In addition, we propose a simple yet efficient proximal-gradient method for optimizing GFlasso that can also be applied to any optimization problems with a convex smooth loss and the general class of fusion penalty defined on arbitrary graph structures. By exploiting the structure of the non-smooth “fusion penalty”, our method achieves a faster convergence rate than the standard first-order method, sub-gradient method, and is significantly more scalable than the widely adopted second-order cone-programming and quadratic-programming formulations. In addition, we provide an analysis of the consistency property of the GFlasso model. Experimental results not only demonstrate the superiority of GFlasso over the standard lasso but also show the efficiency and scalability of our proximal-gradient method.

Keywords: lasso, fused lasso, multi-task learning, structured sparsity, proximal-gradient method

*To whom correspondence should be addressed: epxing@cs.cmu.edu

1 Introduction

In multi-task learning, we are interested in learning multiple related tasks jointly by analyzing data from all of the tasks at the same time instead of considering each task individually [21, 22, 15]. When data are scarce, it is greatly advantageous to borrow the information in the data from other related tasks to learn each task more effectively.

In this paper, we consider a multi-task regression problem, where each task is to learn a functional mapping from a high-dimensional input space to a continuous-valued output space and only a small number of input covariates are relevant to the output. Furthermore, we assume that the outputs are related in a complex manner, and that this output structure is available as prior knowledge in the form of a graph. Given this setting, it is reasonable to believe that closely related outputs tend to share a common set of relevant inputs. Our goal is to recover this structured sparsity pattern in the regression coefficients shared across tasks related through a graph.

When the tasks are assumed to be equally related to inputs without any structure, a mixed-norm regularization such as ℓ_1/ℓ_2 - and ℓ_1/ℓ_∞ -norms has been used to find inputs relevant to all of the outputs jointly [15, 19]. However, in many real-world problems, some of the tasks are often more closely related and more likely to share common relevant covariates than other tasks. Thus, it is necessary to take into account the complex correlation structure in the outputs for a more effective multi-task learning. For example, in genetic association analysis, where the goal is to discover few genetic variants or single nucleotide polymorphisms (SNPs) out of millions of SNPs (inputs) that influence phenotypes (outputs) such as gene expression measurements [23], groups of genes in the same pathways are more likely to share common genetic variants affecting them than other genes. In a neuroscience application, an ℓ_1/ℓ_∞ -regularized multi-task regression has been used to predict neural activities (outputs) in brain in response to words (inputs) [11]. Since neural activities in the brain are locally correlated, it is necessary to take into account this local correlation in different brain regions rather than assuming that all regions share a similar response as in [11]. A similar problem arises in stock prediction where some of the stock prices are more highly correlated than others [6].

The main contributions of this paper are two-fold. First, we propose a structured regularized-regression approach called graph-guided fused lasso (GFlasso) for sparse multi-task learning problems and introduce a novel penalty function based on fusion penalty that encourages tasks related according to the graph to have a similar sparsity pattern. Second, we propose an efficient optimization algorithm based on proximal-gradient method that can be used to solve GFlasso optimization as well as any optimizations with a convex smooth loss and general fusion penalty which can be defined on an arbitrary graph structure.

In addition to the standard lasso penalty for overall sparsity [17], GFlasso employs a “fusion penalty” [18] that fuses regression coefficients across correlated outputs, using the weighted connectivity of the output graph as a guide. The overall effect of the GFlasso penalty is that it allows us to identify a parsimonious set of input factors relevant to dense subgraphs of outputs as illustrated in Figure 1. To the best of our knowledge, this work is the first to consider the graph structure over the outputs in multi-task learning. We also provide an analysis of the consistency property of the GFlasso model.

The fusion penalty that we adopt to construct the GFlasso penalty has been widely used for

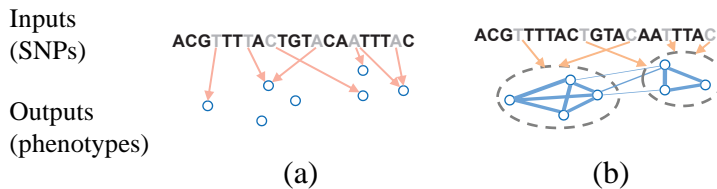


Figure 1: Illustrations of multi-task regression with (a) lasso, (b) graph-guided fused lasso.

sparse learning problems, including fused lasso [18], fused-lasso signal approximator [5], and network learning [10]. However, because of the non-separability of the fusion penalty function, developing a fast optimization algorithm has remained a challenge. The available optimization methods include formulating the problem as second-order cone programming (SOCP) or quadratic programming (QP) and solving them by interior-point methods (IPM) [18], but these approaches are computationally expensive even for problems of moderate size. In order to reduce the computational cost, when the fusion penalty is defined on a chain or two-way grid structure over inputs, the pathwise coordinate optimization has been applied [5]. However, when the fusion penalty is defined on a general graph, this method cannot be easily applied because of the relatively complex sub-gradient representation. In addition, as pointed out in [18], this method “is not guaranteed to yield exact solution” when the design matrix is not orthogonal. Very recently, an unpublished manuscript [8] proposed a different algorithm which reformulates the problem as a maximum flow problem. However, this algorithm works only when the dimension is less than the sample size and hence is not applicable to high-dimensional sparse learning problems. In addition, it lacks any theoretical guarantee of the convergence.

In order to make the optimization efficient and scalable, a first-order method (using only gradient) is desired. In this paper, we propose a proximal-gradient method to solve GFlasso. More precisely, by exploiting the structure of the non-smooth fusion penalty, we introduce its smooth approximation and optimize this approximation based on the accelerated gradient method in [14]. It can be shown that our method achieves the convergence rate of $O(\frac{1}{\epsilon})$, where the ϵ is the desired accuracy. Our method is significantly faster than the most natural first-order method, subgradient method [4] with $O(\frac{1}{\epsilon^2})$ convergence rate and more scalable by orders of magnitude than IPM for SOCP and QP. We emphasize that although we present this algorithm for GFlasso, it can also be applied to solve any regression problems involving a fusion penalty such as fused lasso with a univariate response, where the fusion penalty can be defined on any structures such as chain, grid, or graphs. In addition, it is easy to implement with only a few lines of MATLAB code.

The rest of the paper is organized as follows. In Section 2, we briefly review lasso and ℓ_1/ℓ_2 -regularized regression for sparse multi-task learning. In Section 3, we present GFlasso. In Section 4, we present our proximal-gradient optimization method for GFlasso and other related optimization problems, and discuss its convergence rate and complexity analysis. In Section 5, we present the preliminary consistency result of GFlasso. In Section 6, we demonstrate the performance of the proposed method on simulated and asthma datasets, followed by conclusions in Section 7.

2 Preliminary: ℓ_1 - and ℓ_1/ℓ_2 -Regularized Multi-task Regression

Assume a sample of N instances, each represented by a J -dimensional input vector and a K -dimensional output vector. Let $\mathbf{X} = (\mathbf{x}_1, \dots, \mathbf{x}_J) \in \mathbb{R}^{N \times J}$ denote the input matrix, and let $\mathbf{Y} = (\mathbf{y}_1, \dots, \mathbf{y}_K) \in \mathbb{R}^{N \times K}$ represent the output matrix. For each of the K output variables (so called tasks), we assume a linear model:

$$\mathbf{y}_k = \mathbf{X}\boldsymbol{\beta}_k + \boldsymbol{\epsilon}_k, \quad \forall k = 1, \dots, K, \quad (1)$$

where $\boldsymbol{\beta}_k = (\beta_{1k}, \dots, \beta_{Jk})^T \in \mathbb{R}^J$ is the vector of regression coefficients for the k -th output variable, and $\boldsymbol{\epsilon}_k$ is a vector of N independent zero-mean Gaussian noise. We center the \mathbf{y}_k 's and \mathbf{x}_j 's such that $\sum_{i=1}^N y_{ik} = 0$ and $\sum_{i=1}^N x_{ij} = 0$, and consider the model without an intercept.

Let $\mathbf{B} = (\boldsymbol{\beta}_1, \dots, \boldsymbol{\beta}_K)$ denote the $J \times K$ matrix of regression coefficients of all K response variables. Then, lasso [17] obtains $\widehat{\mathbf{B}}^{\text{lasso}}$ by solving the following optimization problem:

$$\widehat{\mathbf{B}}^{\text{lasso}} = \arg \min_{\mathbf{B}} \frac{1}{2} \|\mathbf{Y} - \mathbf{X}\mathbf{B}\|_F^2 + \lambda \|\mathbf{B}\|_1, \quad (2)$$

where $\|\cdot\|_F$ denotes the matrix Frobenius norm, $\|\cdot\|_1$ denotes the the entry-wise matrix ℓ_1 -norm (i.e., $\|\mathbf{B}\|_1 = \sum_{k=1}^K \sum_{j=1}^J |\beta_{jk}|$) and λ is a regularization parameter that controls the sparsity level. We note that lasso in (2) does not offer any mechanism for a joint estimation of the parameters for the multiple outputs.

Recently, a mixed-norm (e.g., ℓ_1/ℓ_2) regularization has been used for a recovery of joint sparsity across multiple tasks, when the tasks share the common set of relevant covariates [3, 15]. More precisely, it encourages the relevant covariates to be shared across output variables and finds estimates in which only few covariates have non-zero regression coefficients for one or more of the K output variables. The corresponding optimization problem is given as follows:

$$\widehat{\mathbf{B}}^{\ell_1/\ell_2} = \arg \min_{\mathbf{B}} \frac{1}{2} \|\mathbf{Y} - \mathbf{X}\mathbf{B}\|_F^2 + \lambda \|\mathbf{B}\|_{1,2}, \quad (3)$$

where $\|\mathbf{B}\|_{1,2} = \sum_{j=1}^J \|\boldsymbol{\beta}^j\|_2$, $\boldsymbol{\beta}^j$ is the j -th row of the regression coefficient matrix \mathbf{B} , and $\|\cdot\|_2$ denotes the vector ℓ_2 -norm. Although the mixed-norm allows information to be combined across output variables, it assumes all of the tasks are equally related to inputs, and cannot incorporate a complex structure in how the outputs themselves are correlated.

3 Graph-guided Fused Lasso for Sparse Structured Multitask Regression

In this section, we propose GFlasso that explicitly takes into account the complex dependency structure in the output variables represented as a graph while estimating the regression coefficients. We assume that the output structure of the K output variables is available as a graph G with a set

of nodes $V = \{1, \dots, K\}$ and edges E . In this paper, we adopt a simple strategy for constructing such graphs by computing pairwise correlations based on \mathbf{y}_k 's, and connecting two nodes with an edge if their correlation is above a given threshold ρ . More sophisticated methods can be easily employed, but they are not the focus of this paper. Let $r_{ml} \in \mathbb{R}$ denote the weight (can be either positive or negative) of an edge $e = (m, l) \in E$ that represents the strength of correlation between the two nodes. Here, we simply adopt the Pearson's correlation between \mathbf{y}_m and \mathbf{y}_l as r_{ml} .

Given the graph G , it is reasonable to assume that if two output variables are connected with an edge in the graph, they tend to be influenced by the same set of covariates with similar strength. In addition, we assume that the edge weights in the graph G contain information on how strongly the two output variables are related and thus share relevant covariates. GFlasso employs an additional constraint over the standard lasso by fusing the β_{jm} and β_{jl} if $(m, l) \in E$ as follows:

$$\hat{\mathbf{B}}^{\text{GF}} = \min_{\mathbf{B}} f(\mathbf{B}) \equiv \frac{1}{2} \|\mathbf{Y} - \mathbf{X}\mathbf{B}\|_F^2 + \lambda \|\mathbf{B}\|_1 + \gamma \sum_{e=(m,l) \in E} \tau(r_{ml}) \sum_{j=1}^J |\beta_{jm} - \text{sign}(r_{ml})\beta_{jl}|, \quad (4)$$

where λ and γ are regularization parameters that control the complexity of the model. A larger value for γ leads to a greater fusion effect. In this paper, we consider $\tau(r) = |r|$, but any positive monotonically increasing function of the absolute value of correlations can be used. The $\tau(r_{ml})$ weights the fusion penalty for each edge such that β_{jm} and β_{jl} for highly correlated outputs with large $|r_{ml}|$ receive a greater fusion effect than other pairs of outputs with weaker correlations. The $\text{sign}(r_{ml})$ indicates that two negatively correlated outputs are encouraged to have the same set of relevant covariates with the same absolute value of regression coefficients of the opposite sign.

When the edge-level fusion penalty is applied to all of the edges in the entire graph G in the GFlasso penalty, the overall effect is that each subset of output variables within a densely connected subgraph tends to have common relevant covariates. This is because the fusion effect propagates through the neighboring edges, fusing the regression coefficients for each pair of outputs connected by an edge, where the amount of such propagation is determined by the level of local edge connectivities and edge weights.

The idea of using a fusion penalty has been first proposed for the problem with a univariate response and high-dimensional covariates to fuse the regression coefficients of two adjacent covariates when the covariates are assumed to be ordered such as in time [18]. In GFlasso, we employ a similar but more general strategy in a multiple-output regression in order to identify shared relevant covariates for related output variables.

4 Proximal-Gradient Method for Optimization

Although the optimization problem for GFlasso in (4) is convex, it is not trivial to optimize it because of the non-smooth penalty function. The problem can be formulated as either SOCP or QP using the similar strategy in [18]. The state-of-the-art approach for solving SOCP and QP are based on an IPM that requires solving a Newton system to find a search direction. Thus, it is computationally very expensive even for problems of moderate size.

In this section, we propose a proximal-gradient method which utilizes only the first-order information with a fast convergence rate and low computation complexity per iteration. More precisely, we first reformulate the ℓ_1 and fusion penalty altogether into a max problem over the auxiliary variables, and then introduce its smooth lower bound. Instead of optimizing the original penalty, we adopt the accelerated gradient descent method [14] to optimize the smooth lower bound.

The approach of “proximal” method is quite general in that it optimizes a lower or upper bound of the original objective function, rather than optimize the objective function directly. This lower or upper bound has a simpler form that allows for an easy optimization. Recently, different variants of a proximal-gradient method have been applied to solve optimization problems with a convex loss and non-smooth penalty, including matrix completion [9] and sparse signal reconstruction [16]. However, the non-smooth penalties in these works are the norm of the coefficient itself instead of the norm of a linear transformation of the coefficient. So they use a quadratic approximation to the smooth loss function while keeping the easily-handled non-smooth penalty in their original form. In contrast, in this work, we find a smooth lower bound of the complicated non-smooth penalty term.

4.1 A Reformulation of the Non-smooth Penalty Term

First, we rewrite the graph-guided fusion penalty function in (4), using a vertex-edge incident matrix $H \in \mathbb{R}^{K \times |E|}$, as follows:

$$\sum_{e=(m,l) \in E} \tau(r_{ml}) \sum_{j=1}^J |\beta_{jm} - \text{sign}(r_{ml})\beta_{jl}| \equiv \|\mathbf{B}H\|_1,$$

where $H \in \mathbb{R}^{K \times |E|}$ is a variant vertex-edge incident matrix defined as below:

$$H_{k,e} = \begin{cases} \tau(r_{ml}) & \text{if } e = (m, l) \text{ and } k = m \\ -\text{sign}(r_{ml})\tau(r_{ml}) & \text{if } e = (m, l) \text{ and } k = l \\ 0 & \text{otherwise.} \end{cases}$$

Therefore, the overall penalty in (4) including both lasso and graph-guided fusion penalty functions can be written as $\|\mathbf{B}C\|_1$, where $C = (\lambda I, \gamma H)$ and $I \in \mathbb{R}^{K \times K}$ denotes an identity matrix.

Since the dual norm of the entry-wise matrix ℓ_∞ norm is the ℓ_1 norm, we can further rewrite the overall penalty as:

$$\|\mathbf{B}C\|_1 \equiv \max_{\|\mathbf{A}\|_\infty \leq 1} \langle \mathbf{A}, \mathbf{B}C \rangle, \quad (5)$$

where $\langle \mathbf{U}, \mathbf{V} \rangle \equiv \text{Tr}(\mathbf{U}^T \mathbf{V})$ denotes a matrix inner product, $\mathbf{A} \in \mathcal{Q} = \{\mathbf{A} \mid \|\mathbf{A}\|_\infty \leq 1, \mathbf{A} \in \mathbb{R}^{J \times (K+|E|)}\}$ is an auxiliary matrix associated with $\|\mathbf{B}C\|_1$, and $\|\cdot\|_\infty$ is the matrix entry-wise ℓ_∞ norm, defined as the maximum absolute value of all entries in the matrix.

According to (5), the penalty term can be viewed as the inner product of the auxiliary matrix \mathbf{A} and the linear mapping of \mathbf{B} , $\Gamma(\mathbf{B}) \equiv \mathbf{B}C$, where the linear operator Γ is a mapping from $\mathbb{R}^{J \times K}$ into $\mathbb{R}^{J \times (K+|E|)}$. By the fact that $\langle \mathbf{A}, \Gamma(\mathbf{B}) \rangle \equiv \text{Tr}(\mathbf{A}^T \mathbf{B}C) = \text{Tr}(C \mathbf{A}^T \mathbf{B}) \equiv \langle \mathbf{A}C^T, \mathbf{B} \rangle$, the adjoint operator of Γ is $\Gamma^*(\mathbf{A}) = \mathbf{A}C^T$ that maps $\mathbb{R}^{J \times (K+|E|)}$ back into $\mathbb{R}^{J \times K}$. Essentially, the

adjoint operator Γ^* is the linear operator induced by Γ defined in the space of auxiliary variables. The use of the linear mapping Γ and its adjoint Γ^* will simplify our notation and provide a more consistent way to present our key theorem as shown in the next section.

4.2 Proximal-Gradient Method

The formulation of the penalty in (5) is still a non-smooth function in \mathbf{B} , and this makes the optimization still challenging. To tackle this problem, we introduce an auxiliary strongly convex function to construct a smooth approximation of (5). More precisely, we define:

$$f_\mu(\mathbf{B}) = \max_{\|\mathbf{A}\|_\infty \leq 1} \langle \mathbf{A}, \mathbf{BC} \rangle - \mu d(\mathbf{A}), \quad (6)$$

where μ is a positive smoothness parameter and $d(\mathbf{A})$ is an arbitrary smooth strongly-convex function defined on \mathcal{Q} . The original penalty term can be viewed as $f_\mu(\mathbf{B})$ with $\mu = 0$, i.e. $f_0(\mathbf{B}) = \max_{\|\mathbf{A}\|_\infty \leq 1} \langle \mathbf{A}, \mathbf{BC} \rangle$. Since our algorithm will utilize the optimal solution \mathbf{A}^* to (6), we choose $d(\mathbf{A}) \equiv \frac{1}{2} \|\mathbf{A}\|_F^2$ so that we can obtain the closed-form solution for \mathbf{A}^* .

It can be easily seen that $f_\mu(\mathbf{B})$ is a lower bound of $f_0(\mathbf{B})$. To bound the gap between them, let

$$D = \max_{\|\mathbf{A}\|_\infty \leq 1} d(\mathbf{A}) = \frac{1}{2} \|\mathbf{A}\|_F^2 = \frac{1}{2} J(K + |E|). \quad (7)$$

Then, we have $f_0(\mathbf{B}) - f_\mu(\mathbf{B}) \leq \mu D = \mu J(K + |E|)/2$. From the key theorem we present below, we know that $f_\mu(\mathbf{B})$ is a smooth function for any $\mu > 0$. Therefore, $f_\mu(\mathbf{B})$ can be viewed as a smooth approximation of $f_0(\mathbf{B})$ with the maximum gap of μD and the μ controls the gap between $f_\mu(\mathbf{B})$ and $f_0(\mathbf{B})$. As we discuss in the next section in more detail, if our desired accuracy is ϵ , i.e., $f(\mathbf{B}^t) - f(\mathbf{B}^*) \leq \epsilon$, where \mathbf{B}^t is the approximate solution at the t -th iteration, and \mathbf{B}^* is the optimal solution to the objective function in (4), we should set $\mu = \frac{\epsilon}{2D}$ to achieve the best convergence rate.

Now, we present the key theorem to show that $f_\mu(\mathbf{B})$ is smooth and that $\nabla f_\mu(\mathbf{B})$ is Lipschitz continuous. This theorem is also stated in [14] but without a detailed proof of the smoothness property and a derivation of the gradient. We provide a simple proof based on the Fenchel Conjugate and properties of subdifferential. The details of the proof are presented in Appendix.

Theorem 1. *For any $\mu > 0$, $f_\mu(\mathbf{B})$ is a convex and continuously differentiable function in \mathbf{B} with the gradient:*

$$\nabla f_\mu(\mathbf{B}) = \Gamma^*(\mathbf{A}^*) = \mathbf{A}^* \mathbf{C}^T, \quad (8)$$

where Γ^* is the adjoint operator of Γ defined at the end of Section 4.1; \mathbf{A}^* is the optimal solution to (6). Furthermore, the gradient $\nabla f_\mu(\mathbf{B})$ is Lipschitz continuous with the Lipschitz constant $L_\mu = \frac{1}{\mu} \|\Gamma\|^2$, where $\|\Gamma\|$ is the norm of the linear operator Γ defined as $\|\Gamma\| \equiv \max_{\|\mathbf{V}\|_2 \leq 1} \|\Gamma(\mathbf{V})\|_2$.

To compute the $\nabla f_\mu(\mathbf{B})$ and L_μ in the above theorem, we need to know \mathbf{A}^* and $\|\Gamma\|$. We present the closed-form expressions of \mathbf{A}^* and $\|\Gamma\|$ in the following two lemmas. The proof of Lemma 2 is provided in Appendix.

Lemma 1. Let \mathbf{A}^* be the optimal solution of (6):

$$\mathbf{A}^* = S\left(\frac{\mathbf{B}\mathbf{C}}{\mu}\right),$$

where S is the shrinkage operator defined as follows. For $x \in \mathbb{R}$, $S(x) = x$ if $-1 < x < 1$, $S(x) = 1$ if $x \geq 1$, and $S(x) = -1$ if $x \leq -1$. For matrix \mathbf{A} , $S(\mathbf{A})$ is defined as applying S on each and every entry of \mathbf{A} .

Proof. By taking the derivative of (6) over \mathbf{A} and setting it to zeros, we obtain $\mathbf{A} = \frac{\mathbf{B}\mathbf{C}}{\mu}$. Then, we project this solution onto the \mathcal{Q} and get the optimal solution \mathbf{A}^* . \square

Lemma 2. $\|\Gamma\|$ is upper bounded by $\|\Gamma\|_U \equiv \sqrt{\lambda^2 + 2\gamma^2 \max_{k \in V} d_k}$, where

$$d_k = \sum_{e \in E \text{ s.t. } e \text{ incident on } k} (\tau(r_e))^2 \quad (9)$$

for $k \in V$ in graph G ; and this bound is tight.

Given the results in Theorem 1, now we present our proximal-gradient method for GFlasso. We substitute the penalty term in (5) with its smooth approximation $f_\mu(\mathbf{B})$ and obtain the smooth optimization problem:

$$\min_{\mathbf{B}} \tilde{f}(\mathbf{B}) \equiv \frac{1}{2} \|\mathbf{Y} - \mathbf{X}\mathbf{B}\|_2^2 + f_\mu(\mathbf{B}). \quad (10)$$

According to Theorem 1, the gradient of $\tilde{f}(\mathbf{B})$ is:

$$\nabla \tilde{f}(\mathbf{B}) = \mathbf{X}^T(\mathbf{X}\mathbf{B} - \mathbf{Y}) + \mathbf{A}^* \mathbf{C}^T. \quad (11)$$

Note that $\nabla \tilde{f}(\mathbf{B})$ is Lipschitz continuous with the Lipschitz constant L tightly upper bounded by L_U :

$$L = \lambda_{\max}(\mathbf{X}^T \mathbf{X}) + L_\mu \leq \lambda_{\max}(\mathbf{X}^T \mathbf{X}) + \frac{\lambda^2 + 2\gamma^2 \max_{k \in V} d_k}{\mu} \equiv L_U, \quad (12)$$

where $\lambda_{\max}(\mathbf{X}^T \mathbf{X})$ is the largest eigenvalue of $(\mathbf{X}^T \mathbf{X})$.

Instead of optimizing the original function $f(\mathbf{B})$ in (4), we optimize $\tilde{f}(\mathbf{B})$. Since $\tilde{f}(\mathbf{B})$ is a smooth lower bound of $f(\mathbf{B})$, we can adopt the accelerated gradient-descent method, so called Nesterov's method [14], to minimize smooth $\tilde{f}(\mathbf{B})$ as shown in Algorithm 1.

In contrast to the standard gradient-descent algorithm, Algorithm 1 involves the updating of three sequences $\{\mathbf{W}^t\}$, $\{\mathbf{B}^t\}$ and $\{\mathbf{Z}^t\}$, where \mathbf{B}^t is obtained from the gradient-descent update based on \mathbf{W}^t with the stepsize $\frac{1}{L_U}$; \mathbf{Z}^t is the weighted combination of all previous gradient information and \mathbf{W}^{t+1} is the convex combination of \mathbf{B}^t and \mathbf{Z}^t . Intuitively, the reason why this method is superior to the standard gradient descent is that it utilizes all of the gradient information from the first step to the current one for each update, while the standard gradient-descent update is only based on the gradient information at the current step.

Algorithm 1 Proximal-Gradient Method for GFlasso

Input: \mathbf{X} , \mathbf{Y} , λ , γ , graph structure G , desired accuracy ϵ .

Initialization: Construct $C = (\lambda I, \gamma H)$; compute L_U according to (12); compute D in (7) and set $\mu = \frac{\epsilon}{2D}$; set $\mathbf{W}^0 = \mathbf{0} \in \mathbb{R}^{J \times K}$;

Iterate For $t = 0, 1, 2, \dots$ until convergence of \mathbf{B}^t :

1. Compute $\nabla \tilde{f}(\mathbf{W}^t)$ according to (11).
2. Perform the gradient descent step : $\mathbf{B}^t = \mathbf{W}^t - \frac{1}{L_U} \nabla \tilde{f}(\mathbf{W}^t)$.
3. Set $\mathbf{Z}^t = -\frac{1}{L_U} \sum_{i=0}^t \frac{i+1}{2} \nabla \tilde{f}(\mathbf{W}^i)$.
4. Set $\mathbf{W}^{t+1} = \frac{t+1}{t+3} \mathbf{B}^t + \frac{2}{t+3} \mathbf{Z}^t$.

Output: $\hat{\mathbf{B}} = \mathbf{B}^t$

4.3 Complexity

Although we optimize the approximation function \tilde{f} , it still can be proven that the $\hat{\mathbf{B}}$ obtained from Algorithm 1 is sufficiently close to the optimal solution \mathbf{B}^* to the original objective function in (4). We present the convergence rate of Algorithm 1 in the next theorem.

Theorem 2. *Let \mathbf{B}^* be the optimal solution to (4) and \mathbf{B}^t be the intermediate solution at the t -th iteration in Algorithm 1. If we require $f(\mathbf{B}^t) - f(\mathbf{B}^*) \leq \epsilon$ and set $\mu = \frac{\epsilon}{2D}$, then the number of iterations t is upper bounded by:*

$$\sqrt{\frac{4\|\mathbf{B}^*\|_F^2}{\epsilon} \left(\lambda_{\max}(\mathbf{X}^T \mathbf{X}) + \frac{2D\|\Gamma\|_U^2}{\epsilon} \right)}, \quad (13)$$

where D and $\|\Gamma\|$ are as in (7) and Lemma 2 respectively.

The key idea behind the proof is to decompose $f(\mathbf{B}^t) - f(\mathbf{B}^*)$ into 3 parts: (i) $f(\mathbf{B}^t) - \tilde{f}(\mathbf{B}^t)$, (ii) $\tilde{f}(\mathbf{B}^t) - \tilde{f}(\mathbf{B}^*)$, (iii) $\tilde{f}(\mathbf{B}^*) - f(\mathbf{B}^*)$. (i) and (iii) can be bounded by the gap of the approximation μD . Since \tilde{f} is a smooth function, we can bound (ii) by the accuracy bound when applying the accelerated gradient method to minimize smooth functions [14]. We obtain (13) by balancing these three terms. The details of the proof are presented in Appendix. According to Theorem 2, Algorithm 1 converges in $O(\frac{\sqrt{2D}}{\epsilon})$ iterations, which is much faster than the subgradient method with the convergence rate of $O(\frac{1}{\epsilon})$. Note that the convergence rate of our method depends on D through the term $\sqrt{2D}$, which again depends on the problem size with $D = J(K + |E|)/2$.

Theorem 2 suggests that a good strategy for choosing the parameter μ in Algorithm 1 is to set $\mu = \frac{\epsilon}{2D}$, where D is determined by the problem size. Instead of fixing the value for ϵ , we directly set μ or the ratio of ϵ and D to a constant, because this automatically has the effect of scaling ϵ according to the problem size without affecting the quality of the solution.

Assuming that we pre-compute and store $\mathbf{X}^T \mathbf{X}$ and $\mathbf{X}^T \mathbf{Y}$ with the time complexity of $O(J^2 N + JKN)$, the main computational cost is to calculate the gradient $\nabla \hat{f}(\mathbf{W}_t)$ with the time complexity of $O(J^2 K + J|E|)$ in each iteration. Note that the per-iteration complexity of our method is (i) independent of sample size N , which can be very large for large-scale applications, and (ii) linear in the number of edges $|E|$, which can also be large in many cases. In comparison, the second-order method such as SOCP has a much higher complexity per iteration. According to [12], SOCP costs $O(J^2(K + |E|)^2(KN + JK + J|E|))$ per iteration, thus cubic in the number of edges and linear in sample size. Moreover, each IPM iteration of SOCP requires significantly more memory to store the Newton linear system.

4.4 Proximal-Gradient Method for General Fused Lasso

The proximal-gradient method for GFlasso that we presented in the previous section can be easily adopted to efficiently solve any types of optimization problems with a smooth convex loss function and fusion penalties such as fused-lasso regression and fused-lasso signal approximator [18, 8]. We emphasize that our method can be applied to the fusion penalty defined on an arbitrary graph structure, while the widely adopted pathwise coordinate method is only known to be applied to the fusion penalty defined on special graph structures, i.e., chain and two-way grid. For example, the general fused lasso solves a univariate regression problem with a graph fusion penalty as follows:

$$\hat{\boldsymbol{\beta}} = \arg \min_{\boldsymbol{\beta}} \frac{1}{2} \|\mathbf{y} - \mathbf{X}\boldsymbol{\beta}\|_2^2 + \lambda \sum_{j=1}^J |\beta_j| + \gamma \sum_{e=(m,l) \in E} |\beta_m - \beta_l|, \quad (14)$$

where $\|\cdot\|_2$ denotes a vector ℓ_2 -norm, $\mathbf{y} \in \mathbb{R}^N$ is the univariate response vector of length N , $\mathbf{X} \in \mathbb{R}^{N \times J}$ is the input matrix, $\boldsymbol{\beta} \in \mathbb{R}^J$ is the regression coefficient vector, and E is the edge set in graph $G = (V, E)$ with $V = \{1, \dots, J\}$. Note that the fusion penalty defined on inputs ordered in time as a chain (i.e., $\sum_{j=1}^{J-1} |\beta_{j+1} - \beta_j|$) [18] is a special case of the penalty in (14). It is straightforward to apply our proximal-gradient method to solve (14) with only a slight modification of the linear mapping $\Gamma(\boldsymbol{\beta}) \equiv C\boldsymbol{\beta}$ and its adjoint $\Gamma^*(\boldsymbol{\alpha}) \equiv C^T \boldsymbol{\alpha}$.

To the best of our knowledge, the only gradient-based method available for optimizing (14) is the recent work in [8] that adopts a path algorithm. However, this relatively complex algorithm works only for the case of $N > J$, and does not have any theoretical guarantees on convergence. In contrast, our method is more generally applicable, is simpler to implement, and has a faster convergence rate.

5 Asymptotic Consistency Analysis

It is possible to derive results on the asymptotic behavior of the GFlasso estimator that is analogous to the ones in lasso [17] and fused lasso [18] when J and K are fixed as $N \rightarrow \infty$. Assume \mathbf{B} is the true coefficient matrix and $\hat{\mathbf{B}}_N$ is the estimator obtained by optimizing (4). Also assume that the regularization parameter λ_N and γ_N are functions of N . We have the following statistical convergence result:

Theorem 3. If $\lambda_N/\sqrt{N} \rightarrow \lambda_0 \geq 0$, $\gamma_N/\sqrt{N} \rightarrow \gamma_0 \geq 0$ and $C = \lim_{N \rightarrow \infty} \left(\frac{1}{N} \sum_{i=1}^N \mathbf{x}_i \mathbf{x}_i^T \right)$ is non-singular, where \mathbf{x}_i is the i -th row of \mathbf{X} , then

$$\sqrt{N}(\widehat{\mathbf{B}}_N - \mathbf{B}) \rightarrow_d \underset{\mathbf{U}}{\operatorname{argmin}} V(\mathbf{U}), \quad (15)$$

where

$$\begin{aligned} V(\mathbf{U}) = & -2 \sum_k \mathbf{u}_k^T \mathbf{W} + \sum_k \mathbf{u}_k^T C \mathbf{u}_k + \lambda_0^{(1)} \sum_k \sum_j [u_{jk} \operatorname{sign}(\beta_{jk}) I(\beta_{jk} \neq 0) + |u_{jk}| I(\beta_{jk} = 0)] \\ & + \lambda_0^{(2)} \sum_{e=(m,l) \in E} \tau(r_{ml}) \sum_j [u'_{je} \operatorname{sign}(\beta'_{je}) I(\beta'_{je} \neq 0) + |u'_{je}| I(\beta'_{je} = 0)] \end{aligned}$$

with $u'_{je} = u_{jm} - \operatorname{sign}(r_{ml})u_{jl}$ and $\beta'_{je} = \beta_{jm} - \operatorname{sign}(r_{ml})\beta_{jl}$, and \mathbf{W} has an $N(\mathbf{0}, \sigma^2 C)$ distribution.

The proof of the theorem is provided in Appendix.

6 Experiments

In this section, we demonstrate the performance of GFLasso on both simulated and real data, and show the superiority of our proximal-gradient method (Prox-Grad) to the existing optimization methods. Based on our experience for a range of values for μ , we use $\mu = 10^{-4}$ in all of our experiments, since it provided us reasonably good approximation accuracies across problems of different scales. The regularization parameters λ and γ are chosen by cross-validation. The code is written in MATLAB and we terminate our optimization procedure when the relative changes in the objective is below 10^{-6} .

6.1 Simulation Study

6.1.1 Performance of GFLasso on the Recovery of Sparsity

We conduct a simulation study to evaluate the performance of the proposed GFLasso, and compare the results with those from lasso and ℓ_1/ℓ_2 -regularized multi-task regression.

We simulate data using the following scenario analogous to genetic association mapping with $K = 10$, $J = 30$ and $N = 100$. To simulate the input data, we use the genotypes of the 60 individuals from the parents of the HapMap CEU panel, and generate genotypes for additional 40 individuals by randomly mating the original 60 individuals. We generate the regression coefficients β_k 's such that the output y_k 's are correlated with a block-like structure in the correlation matrix. We first choose input-output pairs with non-zero regression coefficients as we describe below. We assume three groups of correlated output variables of sizes 3, 3, and 4. Three relevant inputs are randomly selected for the first group of outputs, and four relevant inputs are selected for each of the other two groups, so that the shared relevant inputs induce correlation among the outputs within each cluster. In addition, we assume another relevant input for outputs in both of the first two

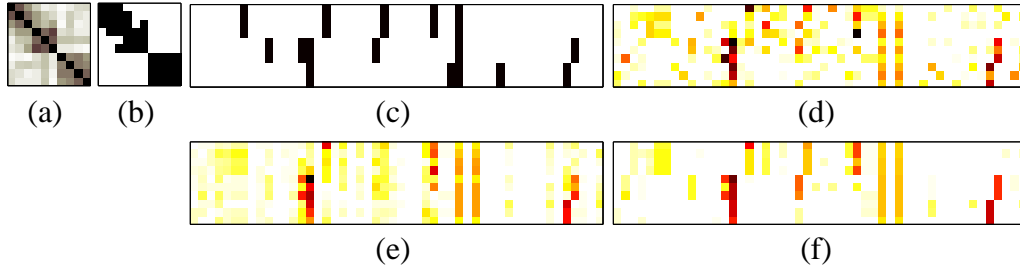


Figure 2: Regression coefficients estimated by different methods based on a single simulated dataset. $b = 0.8$ and threshold $\rho = 0.3$ for the output correlation graph are used. Red pixels indicate large values. (a) The correlation coefficient matrix of phenotypes, (b) the edges of the phenotype correlation graph obtained at threshold 0.3 are shown as white pixels, (c) the true regression coefficients used in simulation. Absolute values of the estimated regression coefficients are shown for (d) lasso, (e) ℓ_1/ℓ_2 -regularized multi-task regression, (f) GFlasso. Rows correspond to outputs and columns to inputs.

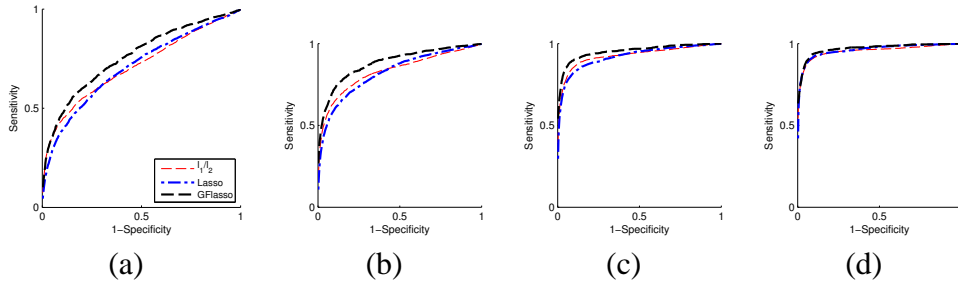


Figure 3: ROC curves for comparing different sparse regression methods with varying signal-to-noise ratios. The b is set to (a) 0.3, (b) 0.5, (c) 0.8, and (d) 1.0.

clusters in order to model the situation of a higher-level correlation structure across two subgraphs. Finally, we assume one additional relevant input for all of the phenotypes. Given the sparsity pattern of \mathbf{B} , we set all non-zero $\beta_{i,j}$ to a constant b to construct the true coefficient matrix \mathbf{B} . Then, we simulate output data based on the linear-regression model with noise distributed as $N(0, 1)$ as in (1), using the simulated genotypes as covariates.

We select the values of the regularization parameters λ and γ by using $(N - 30)$ samples out of the total N samples as a training set, and the remaining 30 samples as a validation set. Then, we use the entire dataset of size N to estimate the final regression coefficients given the selected regularization parameters.

As an illustrative example, a graphical display of the estimated regression coefficients from different methods is shown in Figure 2. It is apparent from Figures 2(d) and (e) that many false positives show up in the results of lasso and ℓ_1/ℓ_2 -regularized multi-task regression. On the other hand, the results from GFlasso in Figure 2(f) show fewer false positives and reveal clear block structures. This experiment suggests that borrowing information across correlated outputs in the output graph as in GFlasso can significantly increase the power of discovering true relevant inputs.

We systematically and quantitatively evaluate the performance of the various methods by computing sensitivity/specificity on the recovered sets of relevant inputs and prediction errors aver-

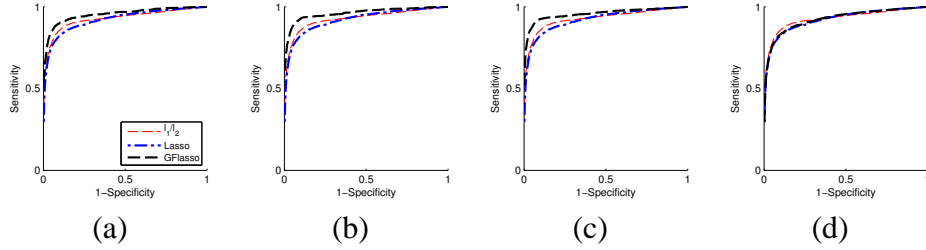


Figure 4: ROC curves for comparison of sparse regression methods with varying thresholds (ρ 's) for output graph structures. (a) $\rho=0.1$, (b) $\rho=0.3$, (c) $\rho=0.5$, and (d) $\rho=0.7$. We use $b = 0.8$ for signal-to-noise ratio.

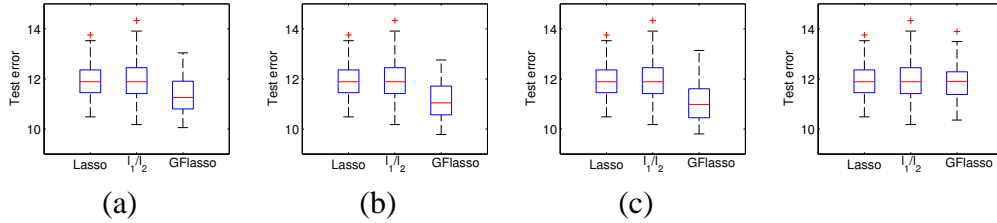


Figure 5: Comparison of multi-task learning methods in terms of prediction error. The threshold ρ for the output correlation graph is (a) $\rho=0.1$, (b) $\rho=0.3$, (c) $\rho=0.5$, and (d) $\rho=0.7$. We use $b = 0.8$ for signal-to-noise ratio.

aged over 50 randomly generated datasets. We generate additional 50 individuals in each training dataset, and compute the prediction error for this test dataset. In order to examine how varying the signal-to-noise ratio affects the performances of the different methods, we simulate datasets with the non-zero elements of the regression coefficient matrix \mathbf{B} set to $b = 0.3, 0.5, 0.8$, and 1.0 , and compute the ROC curves as shown in Figure 3. A threshold of $\rho=0.1$ is used to generate output correlation graphs in GFlasso. We find that GFlasso outperforms the other methods for all of the four chosen signal-to-noise ratios.

Next, we examine the sensitivity of GFlasso to how the output correlation graph is generated, by varying the threshold ρ of edge weights from 0.1 to 0.3, 0.5 and 0.7. With lower values of ρ , more edges would be included in the graph, some of which represent only weak correlations. The purpose of this experiment is to see whether the performance of GFlasso is negatively affected by the presence of these weak and possibly spurious edges that are included due to noise rather than from a true correlation. The results are presented in Figure 4. GFlasso exhibits a greater power than all other methods even at a low threshold $\rho=0.1$. As the threshold ρ increases, the inferred graph structure includes only those edges with significant correlations. When the threshold becomes even higher, e.g., $\rho = 0.7$, the number of edges in the graph becomes close to 0, effectively removing the fusion penalty. As a result, the performances of GFlasso approaches that of lasso, and the two ROC curves almost entirely overlap (Figure 4(d)). Overall, we conclude that when flexible structured methods such as GFlasso are used, taking into account the correlation structure in outputs improves the power of detecting true relevant inputs regardless of the values for ρ . In addition, once the graph contains edges that capture strong correlations, including more edges beyond this point by further lowering the threshold ρ does not significantly affect the performance of GFlasso.

Figure 5 shows the prediction errors using the models learned from the above experiments summarized in Figure 4. It can be seen that GFlasso generally offers a better predictive power than other methods, except for the case where the set of edges for the graph becomes nearly empty due to the high correlation threshold $\rho=0.7$ (Figure 5(d)). In this case, all of methods perform similarly.

6.1.2 Computation Time

In this section, we compare the computation time of our Prox-Grad with those of SOCP and QP formulations for solving GFlasso using simulation data. We use SDPT3 package [20] to solve the SOCP formulation. For the QP formulation, we compare two packages, MOSEK [2] and CPLEX [1], and choose CPLEX since it performs better in terms of computation time. The computation time is reported as the CPU time for one run on the entire training set using the best selected regularization parameters.

To compare the scalability of Prox-Grad with those of SOCP and QP, we vary J , N , K , ρ and present the computation time in seconds in *log-scale* in Figures 6(a)-(d), respectively. All of the experiments are performed on a PC with Intel Core 2 Quad Q6600 CPU 2.4GHz CPU and 4GB RAM. We point out that when we vary the threshold ρ for generating the output graph in Figure 6(d), the increase of ρ decreases the number of edges $|E|$ and hence reduces the computation time. In Figure 6, for large values of J , N , K and small values of ρ , we are unable to collect results for SOCP and QP, because they lead to out-of-memory errors due to the large storage requirement for solving the Newton linear system.

In Figure 6, we find that Prox-Grad is substantially more efficient and can scale up to very high-dimensional and large-scale datasets. QP is more efficient than SOCP since it removes the non-smooth ℓ_1 terms by introducing auxiliary variables for each ℓ_1 term. In addition, we notice that the increase of N does not increase the computation time significantly. This is because N only affects the computation time of $\mathbf{X}^T\mathbf{X}$ and $\mathbf{X}^T\mathbf{y}$, which can be pre-computed, and does not affect the time complexity for each iteration during optimization. This observation is consistent with our complexity analysis in Section 4.3.

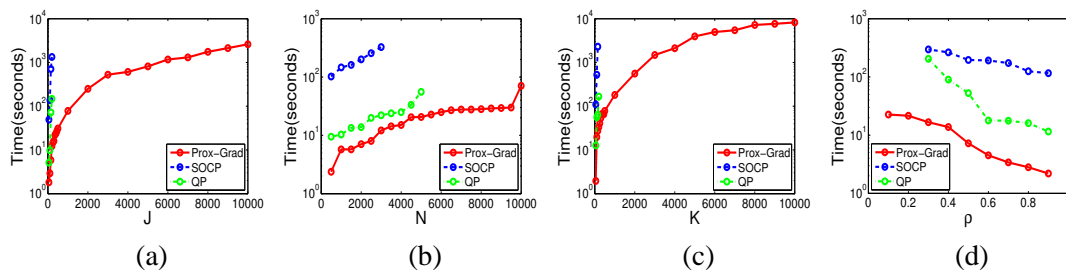


Figure 6: Comparisons of scalabilities of various optimization methods. For Prox-Grad, SOCP and QP, we (a) vary J from 50 to 500 with a step size of 50 and then from 1000 to 10,000 with a step size of 1000, fixing $N = 1000$, $K = 50$ and $\rho = 0.5$, (b) vary N from 500 to 10000 with a step size of 500, fixing $J = 100$, $K = 50$ and $\rho = 0.5$, (c) vary K from 50 to 500 with a step size of 50 and then from 1000 to 10,000 with a step size of 1000, fixing $N = 500$, $J = 100$ and $\rho = 0.5$, and (d) vary ρ from 0.1 to 0.9 with a step size of 0.1, fixing $N = 500$, $J = 100$ and $K = 50$. Note that the y-axis denotes the computation time in seconds in *log-scale*.

6.2 Asthma Dataset

We apply GFlasso to 34 genetic markers and 53 clinical phenotypes collected from 543 asthma patients as a part of the Severe Asthma Research Program (SARP) [13], and compare the results with the ones from lasso and ℓ_1/ℓ_2 -regularized regression. Figure 7(a) shows the correlation matrix of the phenotypes after reordering the variables using the agglomerative hierarchical clustering algorithm so that highly correlated phenotypes are clustered with a block structure along the diagonal. Using the threshold $\rho = 0.7$, we fit the standard lasso, ℓ_1/ℓ_2 -regularized multi-task regression, and GFlasso, and show the estimated β_k 's in Figures 7(c)-(e), with rows and columns representing phenotypes and genotypes respectively. The phenotypes in rows are rearranged according to the ordering given by the agglomerative hierarchical clustering so that each row in Figures 7(c)-(e) is aligned with the phenotypes in the correlation matrix in Figure 7(a). We can see that the vertical bars in the GFlasso estimate in Figure 7(e) span the subset of highly correlated phenotypes that correspond to blocks in Figure 7(a). This block structure is much weaker in the results from the lasso in Figure 7(c), and the blocks tend to span the entire set of phenotypes in the results from the ℓ_1/ℓ_2 -regularized multi-task regression in Figure 7(d).

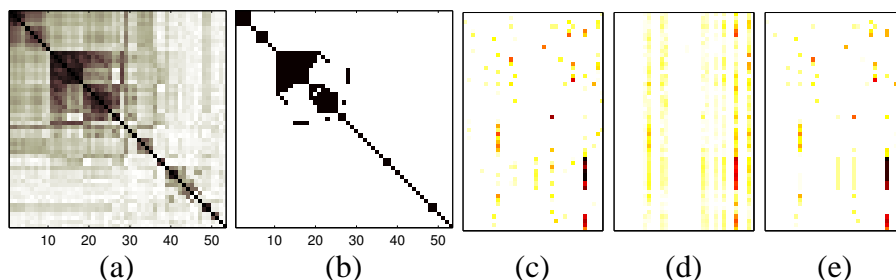


Figure 7: Results for the association analysis of the asthma dataset. (a) Phenotype correlation matrix. (b) Phenotype correlation matrix thresholded at $\rho = 0.7$. (c) lasso; (d) ℓ_1/ℓ_2 -regularized multi-task regression, and (e) GFlasso.

7 Conclusions

In this paper, we discuss a new method called GFlasso for structured multi-task regression that exploits the correlation information in the output variables during the estimation of regression coefficients. GFlasso used a weighted graph structure as a guide to find the set of relevant covariates that jointly affect highly correlated outputs. In addition, we propose an efficient optimization algorithm based on a proximal-gradient method that can be used to solve GFlasso as well as any optimization problems involving a smooth convex loss and fusion penalty defined on arbitrary graph structures. Using simulated and asthma datasets, we demonstrate that including richer information about output structure as in GFlasso improves the performance for discovering true relevant inputs, and that our proximal-gradient method is orders-of-magnitude faster and more scalable than the standard optimization techniques such as QP and SOCP.

Appendix

A.1 Proof of Theorem 1

The $f_\mu(\mathbf{B})$ is a convex function since it is the maximum of a set of functions linear in \mathbf{B} .

For the smoothness property, let the function d^* be the Fenchel conjugate of the distance function d which is defined as:

$$d^*(\Theta) = \max_{\mathbf{A} \in \mathcal{Q}} \langle \mathbf{A}, \Theta \rangle - d(\mathbf{A}). \quad (16)$$

We want to prove d^* is differentiable everywhere by showing that the subdifferential ∂d^* of d^* is a singleton set for any Θ .

By the definition in (16), we have, for any Θ and any $\mathbf{A} \in \mathcal{Q}$:

$$d^*(\Theta) + d(\mathbf{A}) \geq \langle \mathbf{A}, \Theta \rangle, \quad (17)$$

and the inequality holds as an equality if and only if $\mathbf{A} = \arg \max_{\mathbf{A}' \in \mathcal{Q}} \langle \mathbf{A}', \Theta \rangle - d(\mathbf{A}')$.

By the fact that for a convex and smooth function, the conjugate of the conjugate of a function is the function itself (Chapter E in [7]), we have $d^{**} \equiv d$. Then, (17) can be written as:

$$d^*(\Theta) + d^{**}(\mathbf{A}) \geq \langle \mathbf{A}, \Theta \rangle, \quad (18)$$

and the inequality holds as an equality if and only if $\Theta = \arg \max_{\Theta' \in \mathbb{R}^J} \langle \mathbf{A}, \Theta' \rangle - d^*(\Theta')$.

Since (17) and (18) are equivalent, we know that $\mathbf{A} = \arg \max_{\mathbf{A}' \in \mathcal{Q}} \langle \mathbf{A}', \Theta \rangle - d(\mathbf{A}')$ if and only if $\Theta = \arg \max_{\Theta' \in \mathbb{R}^J} \langle \mathbf{A}, \Theta' \rangle - d^*(\Theta')$. The latter equality implies that for any Θ' :

$$d^*(\Theta') \geq d^*(\Theta) + \langle \mathbf{A}, \Theta' - \Theta \rangle,$$

which further means that \mathbf{A} is a subgradient of d^* at Θ by the definition of subgradient.

Summarizing the above arguments, we conclude that \mathbf{A} is a subgradient of d^* at Θ if and only if

$$\mathbf{A} = \arg \max_{\mathbf{A}' \in \mathcal{Q}} \langle \mathbf{A}', \Theta \rangle - d(\mathbf{A}'). \quad (19)$$

Since d is a strongly convex function, this maximization problem in (19) has a unique optimal solution, which means the subdifferential ∂d^* of d^* at any point Θ is a singleton set that contains only \mathbf{A} . Therefore, d^* is differentiable everywhere (Chapter D in [7]) and \mathbf{A} is its gradient:

$$\nabla d^*(\Theta) = \mathbf{A} = \arg \max_{\mathbf{A}' \in \mathcal{Q}} \langle \mathbf{A}', \Theta \rangle - d(\mathbf{A}'). \quad (20)$$

Now we return to our original problem of $f_\mu(\mathbf{B})$ and rewrite it as:

$$f_\mu(\mathbf{B}) = \max_{\mathbf{A} \in \mathcal{Q}} \langle \mathbf{A}, \Gamma(\mathbf{B}) \rangle - \mu d(\mathbf{A}) = \mu \max_{\mathbf{A} \in \mathcal{Q}} \left[\left\langle \mathbf{A}, \frac{\Gamma(\mathbf{B})}{\mu} \right\rangle - d(\mathbf{A}) \right] = \mu d^* \left(\frac{\Gamma(\mathbf{B})}{\mu} \right).$$

Utilizing (20) and the chain rule, we know that $f_\mu(\mathbf{B})$ is continuously differentiable and its gradient takes the following form:

$$\begin{aligned} \nabla f_\mu(\mathbf{B}) &= \mu \Gamma^* \left(\nabla d^* \left(\frac{\Gamma(\mathbf{B})}{\mu} \right) \right) = \mu \Gamma^* \left(\arg \max_{\mathbf{A}' \in \mathcal{Q}} \left[\left\langle \mathbf{A}', \frac{\Gamma(\mathbf{B})}{\mu} \right\rangle - d(\mathbf{A}') \right] \right) \\ &= \Gamma^* \left(\arg \max_{\mathbf{A}' \in \mathcal{Q}} \left[\langle \mathbf{A}', \Gamma(\mathbf{B}) \rangle - \mu d(\mathbf{A}') \right] \right) = \Gamma^*(\mathbf{A}^*). \end{aligned}$$

For the proof of Lipschitz constant of $f_\mu(\mathbf{B})$, readers can refer to [14].

A.2 Proof of Lemma 2

According to the definition of $\|\Gamma\|$, we have:

$$\begin{aligned}\|\Gamma\| &\equiv \max_{\|\mathbf{B}\|_F=1} \|\Gamma(\mathbf{B})\|_F = \max_{\|\mathbf{B}\|_F=1} \|(\lambda\mathbf{B}, \gamma\mathbf{B}H)\|_F \\ &= \max_{\|\mathbf{B}\|_F=1} \sqrt{\lambda^2\|\mathbf{B}\|_F^2 + \gamma^2\|\mathbf{B}H\|_F^2} = \max_{\|\mathbf{B}\|_F=1} \sqrt{\lambda^2 + \gamma^2\|\mathbf{B}H\|_F^2}\end{aligned}$$

Therefore, to bound $\|\Gamma\|$, we only need to find an upper bound for $\max_{\|\mathbf{B}\|_F=1} \|\mathbf{B}H\|_F^2$. According to the formulation of matrix H , we have

$$\|\mathbf{B}H\|_F^2 = \sum_{e=(m,l)\in E} (\tau(r_{ml}))^2 \sum_j (\beta_{jm} - \text{sign}(r_{ml})\beta_{jl})^2 \quad (21)$$

It is well known that $(a - b)^2 \leq 2a^2 + 2b^2$ and the inequality holds as equality if and only if $a = -b$. Using this simple inequality, for each edge $e = (m, l) \in E$, the summation $\sum_j (\beta_{jm} - \text{sign}(r_{ml})\beta_{jl})^2$ is upper-bounded by $\sum_j (2\beta_{jm}^2 + 2\beta_{jl}^2) = 2\|\boldsymbol{\beta}_m\|_2^2 + 2\|\boldsymbol{\beta}_l\|_2^2$. Here, the vectors $\boldsymbol{\beta}_m$ and $\boldsymbol{\beta}_l$ are the m -th and l -th columns of \mathbf{B} . The right-hand side of (21) can be further bounded as:

$$\begin{aligned}\|\mathbf{B}H\|_F^2 &\leq \sum_{e=(m,l)\in E} 2(\tau(r_{ml}))^2 (\|\boldsymbol{\beta}_m\|_2^2 + \|\boldsymbol{\beta}_l\|_2^2) \\ &= \sum_{k\in V} (\sum_{e \text{ incident on } k} 2(\tau(r_e))^2) \|\boldsymbol{\beta}_k\|_2^2 \\ &= \sum_{k\in V} 2d_k \|\boldsymbol{\beta}_k\|_2^2,\end{aligned}$$

where d_k is defined in (9). Note that the first inequality is tight, and that the first equality can be obtained simply by changing the order of summations.

By the definition of Frobenius norm, $\|\mathbf{B}\|_F^2 = \sum_k \|\boldsymbol{\beta}_k\|_2^2$. Hence,

$$\max_{\|\mathbf{B}\|_F=1} \|\mathbf{B}H\|_F^2 \leq \max_{\|\mathbf{B}\|_F=1} \sum_k 2d_k \|\boldsymbol{\beta}_k\|_2^2 = 2 \max_k d_k,$$

where the maximum is achieved by setting the $\boldsymbol{\beta}_k$ corresponding to the largest d_k to be a unit vector and setting other $\boldsymbol{\beta}_k$'s to be zero vectors.

In summary, $\|\Gamma\|$ can be tightly upper bounded as:

$$\begin{aligned}\|\Gamma\| &= \max_{\|\mathbf{B}\|_F=1} \|\Gamma(\mathbf{B})\|_F \\ &= \max_{\|\mathbf{B}\|_F=1} \sqrt{\lambda^2 + \gamma^2\|\mathbf{B}H\|_F^2} \\ &= \sqrt{\lambda^2 + \gamma^2 \max_{\|\mathbf{B}\|_F=1} \|\mathbf{B}H\|_F^2} \\ &\leq \sqrt{\lambda^2 + 2\gamma^2 \max_k d_k} \equiv \|\Gamma\|_U.\end{aligned}$$

A.3 Proof of Theorem 2

Based on Theorem 2 in [14], we have the following lemma:

Lemma 3. *Assume that function $\tilde{f}(\mathbf{B})$ is an arbitrary convex smooth function and its gradient $\nabla \tilde{f}(\mathbf{B})$ is Lipschitz continuous with the Lipschitz constant L that is further upper-bounded by L_U . Apply Algorithm 1 to minimize $\tilde{f}(\mathbf{B})$ and let \mathbf{B}^t be the approximate solution at the t -th iteration. For any \mathbf{B} , we have the following bound:*

$$\tilde{f}(\mathbf{B}^t) - \tilde{f}(\mathbf{B}) \leq \frac{2L_U \|\mathbf{B}\|_F^2}{t^2}. \quad (22)$$

Based on Lemma 3, we present our proof. Recall that the smooth approximation of the function $f(\mathbf{B})$, $\tilde{f}(\mathbf{B})$, is defined as:

$$\tilde{f}(\mathbf{B}) \equiv \frac{1}{2} \|\mathbf{Y} - \mathbf{X}\mathbf{B}\|_F^2 + f_\mu(\mathbf{B}) = \frac{1}{2} \|\mathbf{Y} - \mathbf{X}\mathbf{B}\|_F^2 + \max_{\mathbf{A} \in \mathcal{Q}} \langle \mathbf{A}, \mathbf{B}\mathbf{C} \rangle - \frac{1}{2} \|\mathbf{A}\|_F^2.$$

Since Algorithm 1 optimizes the smooth function $\tilde{f}(\mathbf{B})$, according to Lemma 3, we have

$$\tilde{f}(\mathbf{B}^t) - \tilde{f}(\mathbf{B}^*) \leq \frac{2L_U \|\mathbf{B}^*\|_F^2}{t^2}, \quad (23)$$

where $L_U = \lambda_{\max}(\mathbf{X}^T \mathbf{X}) + \frac{\|\Gamma\|_U^2}{\mu}$ is the upper bound of the Lipschitz constant for $\nabla \tilde{f}(\mathbf{B})$.

We want to utilize the bound in (23); so we decompose $f(\mathbf{B}^t) - f(\mathbf{B}^*)$ into three terms:

$$f(\mathbf{B}^t) - f(\mathbf{B}^*) = \left(f(\mathbf{B}^t) - \tilde{f}(\mathbf{B}^t) \right) + \left(\tilde{f}(\mathbf{B}^t) - \tilde{f}(\mathbf{B}^*) \right) + \left(\tilde{f}(\mathbf{B}^*) - f(\mathbf{B}^*) \right). \quad (24)$$

According to the definition of \tilde{f} , we know that for any \mathbf{B} ,

$$\tilde{f}(\mathbf{B}) \leq f(\mathbf{B}) \leq \tilde{f}(\mathbf{B}) + \mu D,$$

where $D \equiv \max_{\mathbf{A} \in \mathcal{Q}} d(\mathbf{A})$. Therefore, the first term in (24), $f(\mathbf{B}^t) - \tilde{f}(\mathbf{B}^t)$, is upper-bounded by μD ; and the last term in (24) is less than or equal to 0, i.e. $\tilde{f}(\mathbf{B}^*) - f(\mathbf{B}^*) \leq 0$. Combining (23) with these two simple bounds, we have:

$$f(\mathbf{B}^t) - f(\mathbf{B}^*) \leq \mu D + \frac{2L \|\mathbf{B}^*\|_F^2}{t^2} \leq \mu D + \frac{2\|\mathbf{B}^*\|_F^2}{t^2} \left(\frac{\|\Gamma\|_U^2}{\mu} + \lambda_{\max}(\mathbf{X}^T \mathbf{X}) \right). \quad (25)$$

By setting $\mu = \frac{\epsilon}{2D}$ and plugging it into the right hand side of (25), we obtain

$$f(\mathbf{B}^t) - f(\mathbf{B}^*) \leq \frac{\epsilon}{2} + \frac{2\|\mathbf{B}^*\|_F^2}{t^2} \left(\frac{2D\|\Gamma\|_U^2}{\epsilon} + \lambda_{\max}(\mathbf{X}^T \mathbf{X}) \right). \quad (26)$$

If we require the right-hand side of (26) to be equal to ϵ and solve for t , we obtain the bound of t in (13).

Note that we can set $\mu = \frac{\epsilon}{h}$ for any $h > 1$ to achieve $O\left(\frac{1}{\epsilon}\right)$ convergence rate, which is different from (13) only by a constant factor.

A.4 Proof of Theorem 3

Define $V_N(\mathbf{U})$ by

$$\begin{aligned} V_N(\mathbf{U}) = & \sum_{k=1}^K \sum_{i=1}^N [(\varepsilon_{ik} - \mathbf{u}_k^T \mathbf{x}_i / \sqrt{N})^2 - \varepsilon_{ik}^2] + \lambda_N^{(1)} \sum_k \sum_j [|\beta_{jk} + u_{jk} / \sqrt{N}| - |\beta_{jk}|] \\ & + \lambda_N^{(2)} \sum_{(m,l)} f(r_{m,l}) \sum_j [|\beta'_{j,(m,l)} + u'_{j,(m,l)} / \sqrt{N}| - |\beta'_{j,(m,l)}|], \end{aligned}$$

Note that $V_N(\mathbf{u})$ is minimized at $\sqrt{N}(\widehat{\mathbf{B}}_N - \mathbf{B})$. Notice that we have

$$\begin{aligned} & \sum_{k=1}^K \sum_{i=1}^N [(\varepsilon_{ik} - \mathbf{u}_k^T \mathbf{x}_i / \sqrt{N})^2 - \varepsilon_{ik}^2] \rightarrow_d -2 \sum_k [\mathbf{u}_k^T \mathbf{W} + \mathbf{u}_k^T C \mathbf{u}_k], \\ & \lambda_N^{(1)} \sum_k \sum_j [|\beta_{jk} + u_{jk} / \sqrt{N}| - |\beta_{jk}|] \rightarrow_d \lambda_0^{(1)} \sum_k \sum_j [u_{jk} \text{sign}(\beta_{jk}) I(\beta_{jk} \neq 0) + |u_{jk}| I(\beta_{jk} = 0)], \\ & \gamma_N^{(2)} \sum_{e=(m,l) \in E} f(r_{ml}) \sum_j [|\beta'_{je} + u'_{je} / \sqrt{N}| - |\beta'_{je}|] \\ & \rightarrow_d \lambda_0^{(2)} \sum_{e=(m,l) \in E} f(r_{ml}) \sum_j [u'_{je} \text{sign}(\beta'_{je}) I(\beta'_{je} \neq 0) + |u'_{je}| I(\beta'_{je} = 0)]. \end{aligned}$$

Thus, $V_N(\mathbf{U}) \rightarrow_d V(\mathbf{U})$ with the finite-dimensional convergence holding trivially. Since V_N is convex and V has a unique minimum, it follows that $\text{argmin}_{\mathbf{U}} V_N(\mathbf{U}) = \sqrt{N}(\widehat{\mathbf{B}} - \mathbf{B}) \rightarrow_d \text{argmin}_{\mathbf{U}} V(\mathbf{U})$.

References

- [1] *CPLEX 9.0 User's Manual*.
- [2] *The MOSEK Optimization Software* (<http://www.mosek.com/>).
- [3] Andreas Argyriou, Theodoros Evgeniou, and Massimiliano Pontil. Convex multi-task feature learning. *Machine Learning*, 73:243–272, 2006.
- [4] Dimitri Bertsekas. *Nonlinear Programming*. Athena Scientific, 1999.
- [5] Jerome Friedman, Trevor Hastie, Holger Höfling, and Robert Tibshirani. Pathwise coordinate optimization. *Ann. Appl. Stat.*, 1:302–332, 2007.
- [6] Joumana Ghosn and Yoshua Bengio. Multi-task learning for stock selection. In *Advances in Neural Information Processing Systems (NIPS)*, 1997.
- [7] Jean-Baptiste Hiriart-Urruty and Claude Lemarechal. *Fundamentals of Convex Analysis*. Springer, 2001.
- [8] Holger Hoefling. A path algorithm for the fused lasso signal approximator. arXiv:0910.0526v1 [stat.CO].
- [9] Shuiwang Ji and Jieping Ye. An accelerated gradient method for trace norm minimization. In *International Conference on Machine Learning*, 09.
- [10] Mladen Kolar, Le Song, and Eric P. Xing. Sparsistent learning of varying coefficient models with structural changes. In *Advances in Neural Information Processing Systems*, 2009.
- [11] Han Liu, Mark Palatucci, and Jian Zhang. Blockwise coordinate descent procedures for the multi-task lasso, with applications to neural semantic basis discovery. In *International Conference on Machine Learning*, 2009.
- [12] Miguel Sousa Lobo, Lieven Vandenbergh, Stephen Boyd, and Herve Lebert. Applications of second-order cone programming. *Linear Algebra and Its Applications*, 284:193–228, 1998.
- [13] W. Moore, E. Bleeker, D. Curran-Everett, S. Erzurum, B. Ameredes, L. Bacharier, W. Calhoun, M. Castro, K. Chung, and M. Clark. Characterization of the severe asthma phenotype by the National Heart, Lung, and Blood Institute's Severe Asthma Research Program. *Journal of Allergy and Clinical Immunology*, 119:405–13, 2007.
- [14] Yurii Nesterov. Smooth minimization of non-smooth functions. *Mathematical Programming*, 103(1):127–152, 2005.
- [15] Guillaume Obozinski, Ben Taskar, and Michael I. Jordan. High-dimensional union support recovery in multivariate regression. In *NIPS*. MIT Press, 2009.

- [16] Liang Sun, Jun Liu, Jianhui Chen, and Jieping Ye. Efficient recovery of jointly sparse vectors. In *NIPS*, 09.
- [17] Robert Tibshirani. Regression shrinkage and selection via the lasso. *J.R.Statist.Soc.B*, 58:267–288, 1996.
- [18] Robert Tibshirani and Michael Saunders. Sparsity and smoothness via the fused lasso. *J.R.Statist.Soc.B*, 67(1):91–108, 2005.
- [19] Berwin Turlach, William Venables, and Stephen Wright. Simultaneous variable selection. *Technometrics*, 47:349–363, 2005.
- [20] Reha H. Tütüncü, Kim C. Toh, and Michael J. Todd. Solving semidefinite-quadratic-linear programs using sdpt3. *Mathematical Programming Ser. B*, 95:189–217, 2003.
- [21] Kai Yu, Volker Tresp, and Anton Schwaighofer. Learning gaussian processes from multiple tasks. In *International Conference on Machine Learning*, 2005.
- [22] Jian Zhang, Zoubin Ghahramani, and Yiming Yang. Flexible latent variable models for multi-task learning. *Machine Learning*, 73(3):221–242, 2008.
- [23] J. Zhu, B. Zhang, E.N. Smith, B. Drees, R.B. Brem, L. Kruglyak, R.E. Bumgarner, and E.E. Schadt. Integrating large-scale functional genomic data to dissect the complexity of yeast regulatory networks. *Nature Genetics*, 40:854–61, 2008.